Three-Dimensional Wing/Jet Interaction Analysis including Jet Distortion Influences

C. A. Shollenberger*
McDonnell Douglas Research Laboratories, St. Louis, Mo.

Analysis of the interaction of wings with regions of high-energy flow in a uniform stream is motivated by the requirement to predict the aerodynamic characteristics of powered lift systems. The present formulation of the wing/jet problem includes jet deflection and distortion effects. Each jet boundary and wing is replaced by equivalent flow singularities embedded in a uniform stream. The singularity strengths and locations cannot be obtained directly since the jet position is unknown; therefore, an iterative solution technique is employed. Example calculations are presented and comparisons of current solutions are made with previous analyses and experiments.

Nomenclature

A = aspect ratio
b = wing span
C = wing influence coefficient matrix
C_L = wing lift coefficient
C_ℓ = section lift coefficient
C_T = thrust coefficient
E = convergence parameter
e = unit vector
F = force on wing panel
H = total pressure
ℓ = unit vector along vortex filament
l = section lift, vortex filament length
N = number of jet boundary panels
n = unit vector normal to wing surface
p = static surface pressure
S = actuator disk frontal area
T = thrust on actuator disk
U = freestream velocity
V = flow velocity
$\bar{V}$ = mean flow speed
x,y,z = Cartesian coordinates
α = angle of attack
Γ = vortex filament circulation
γ = jet vortex strength
ζ = coordinate normal to surface
η = coordinate perpendicular to local flow and tangent to jet surface
ξ = coordinate parallel to local flow
ρ = fluid density
ϕ = velocity potential

Superscripts

ν = iteration number
1 = resulting from wing
2 = resulting from jet
3 = resulting from freestream

Subscripts

f = flap
i = panel number
j = jet flow
o = outer flow
w = wing
ζ = vector component in ζ direction
η = vector component in η direction
ξ = vector component in ξ direction

Presented as Paper 73-655 at the AIAA 6th Fluid and Plasma Dynamics Conference, Palm Springs, California, July 16-18, 1973; submitted August 6, 1973; revision received October 24, 1974. This research was conducted under the McDonnell Douglas Independent Research and Development Program.

Index categories: Aircraft Aerodynamics (including Components Aerodynamics); Jets, Wakes, and Viscid-Inviscid Flow Interactions; Subsonic and Transonic Flow.

*Research Scientist, Flight Sciences Department; now with Douglas Aircraft Company, Long Beach, California, Member AIAA.

Introduction

PREDICTION of the aerodynamic characteristics of powered high-lift applications requires analysis of the interaction of wings with regions of high-energy flow embedded in a uniform stream. Examples of this class of flows include propeller/wing combinations, ducted fans, externally blown flaps, fan-in-wing, and lift fan configurations. Each of these examples involves jets interacting with solid bodies.

References 1-5 are typical of the propeller slipstream analyses. The usual assumptions of small jet perturbation velocity and small jet deflection and deformation allow linearized analysis but ignore effects that are potentially important to many applications. Reference 6 attempts to include the jet deflection effects by calculation of a jet centerline trajectory. However, this is a rather crude method of estimating jet deflection and ignores the deformation of the jet cross section which could be as important as the jet deflection. Furthermore, the jet boundary condition of Ref. 6 is linearized for uniform jet velocity. In Refs. 7-9 it is shown that a jet, represented by vortex filaments positioned in the direction of the jet flow, rolls up into shapes similar to those observed in experiments. These representations, however, do not completely model the jet vorticity by the trailing vortex filaments. Further, the one-pass procedure used to determine the jet trajectory only approximates the correct vortex filament locations.

A combined jet and wing model has been developed by Rubbert[10] and Monical[11] for the fan-in-wing configuration. The jet trajectory is determined from empirical results, considerably simplifying the calculation since assumption of the jet position eliminates one of the boundary conditions along the jet boundary. In applications where the jet deflection and distortion are dependent on a neighboring wing, the model of Refs. 10 and 11 will not reflect the interdependence of the wing and jet.

Another important class of jet/wing interaction analyses is jet flap theory which considers a thin, high-speed jet issuing from a wing trailing edge. Analyses such as Refs. 12 and 13 consider the idealized model of zero jet thickness and infinite jet velocity. The dynamic jet boundary condition derived from the pressure across the jet necessary to turn the jet, is linearized for small angles and the jet position is assumed to simplify the calculation. Excellent agreement has been obtained between jet flap predictions and experiments even for large jet deflections.

The present formulation of the wing/jet problem accounts for the nonlinear effects of jet deflection and distortion and for nonuniform jet velocity. The method is similar in some aspects to the two-dimensional investigation of the jet/airfoil interaction of Ref. 14 but is complicated significantly by the additional dimension of space. Wings and jets are replaced by equivalent flow singularities, and appropriate boundary conditions are applied to determine the singularity strengths and the jet position. The unknown jet location necessitates an iterative solution technique to successively approximate the wing/jet system until all wing and jet boundary conditions are satisfied. The analysis presented below is a summary of the study presented in Ref. 15.

Analysis

Assumptions

Previous analyses of jets in a uniform freestream flow have mainly considered inviscid and incompressible fluids, an idealization which apparently describes the real flow with reasonable accuracy, especially in the near field of the origin of the jet. In the present study, perfect fluid assumptions will be employed first, with possible later extensions to real fluids. The present effort focuses on the effects of jet deflection and distortion which have not been previously analyzed even for perfect fluids.

Field Equations and Boundary Conditions

The flowfield of the wing/jet problem is composed of regions of fluid at various total pressures separated by jet boundaries and actuator disks. Since the upstream flow is uniform and the fluid is inviscid, all regions of the flowfield are irrotational and a velocity potential can be defined in the outer ambient flow by

$$V_o = \nabla \phi_o \tag{1}$$

Similarly in each jet region

$$V_j = \nabla \phi_j \tag{2}$$

The fluid in all regions is assumed to be incompressible, and hence by the incompressible continuity equation, the outer and jet flows have Laplacian velocity potentials

$$\nabla^2 \phi_o = 0 \tag{3}$$

and

$$\nabla^2 \phi_j = 0 \tag{4}$$

Equations (3) and (4) are the field equations for the flow.

Since solid surfaces such as wings may be in the flowfield, the usual inviscid boundary condition of no flow through such surfaces is applied at all solid boundaries or

$$(\partial \phi_o / \partial \zeta) = 0 \tag{5}$$

when the surface is in the outer flow and

$$(\partial \phi_j / \partial \zeta) = 0 \tag{6}$$

when the surface is within a jet region. Hence ζ is the coordinate locally normal to the solid surface.

In addition to Eqs. (5) and (6), boundary conditions must be applied along the jet boundaries separating the regions of flow with different total pressure. For inviscid flow, jet boundaries are surfaces through which there is no passage of fluid and across which there is a jump in total pressure. Hence one boundary condition on the jet boundaries requires tangential flow along these surfaces.

$$(\partial \phi / \partial \zeta) = 0 \tag{7}$$

where ζ again is the coordinate normal to the jet boundary.

A second jet boundary condition results from the total pressure discontinuity between the jet and freestream flows along the jet boundaries; the static pressure is continuous across the jet boundaries. The discontinuity in total pressure causes a jump in tangential velocity, as seen in Ref. 12 for the two-dimensional case. A jump in tangential velocity across the surface indicates that the jet boundary can be exactly represented by vortex sheets, with the vortex strength related to the total pressure difference between the jet and freestream. Unlike the two-dimensional case, both the direction of the jet boundary vortex filaments and the vortex strength of the filaments are unknown in the three-dimensional problem. In two dimensions the vortex filaments are directed normal to the plane of the flow, whereas in three dimensions the jet boundary vortex filaments are known only to run along the jet boundary surface as indicated in Fig. 1.

At each point along the jet boundary surface the local mean velocity vector is by definition the average of the jet and outer velocity or

$$\bar{V} = (V_o + V_j)/2 \tag{8}$$

A locally orthogonal coordinate system ξ, η, ζ is indicated in Fig. 1. The ξ-axis is parallel to the mean local velocity vector, $\bar{V}$, at a point on the jet boundary, whereas the η-axis is perpendicular to the ξ-axis but within the plane of local tangency to the jet boundary surface. Finally, the ζ-coordinate is normal to the surface with positive direction outward from the jet boundary. Thus if $\bar{V}$ is the magnitude of the mean velocity vector

$$\bar{V} = \bar{V} \boldsymbol{e}_\xi \tag{9}$$

where $\boldsymbol{e}_\xi$ is the unit vector in the ξ direction.

Since the jet boundary vortex strength is a vector quantity in the plane locally tangent to the jet boundary, it may be expressed as the vector sum

$$\gamma = \gamma_\xi \boldsymbol{e}_\xi + \gamma_\eta \boldsymbol{e}_\eta \tag{10}$$

Furthermore, since the vortex sheet represents a discontinuity in the tangential velocity at each point along the jet boundary and the vortex strength is proportional to the jump in velocity between the jet and outer flow regions

$$\gamma = \boldsymbol{e}_\zeta \times (V_o - V_j) \tag{11}$$

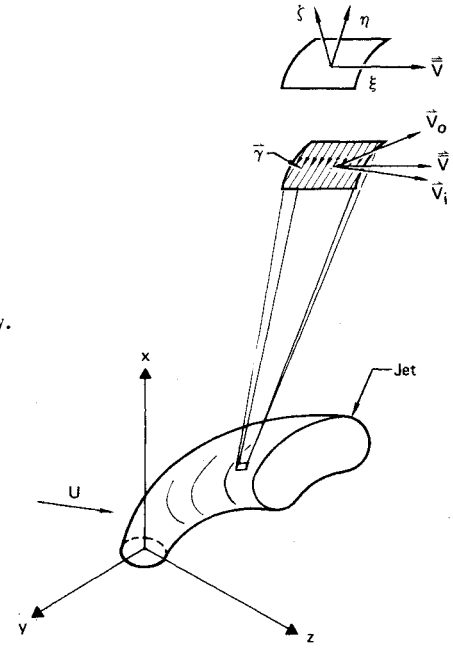

Fig. 1 Jet boundary.

Now V_o and V_j can also be expressed in terms of the vortex strength components and the mean local flow speed by using Eqs. (9-11)

$$V_o = (\bar{V} + \gamma_\eta/2)e_\xi - (\gamma_\xi/2)e_\eta \tag{12}$$

and

$$V_j = (\bar{V} - \gamma_\eta/2)e_\xi + (\gamma_\xi/2)e_\eta \tag{13}$$

To obtain a second boundary condition in addition to Eq. (7) along the jet surfaces, the Bernoulli equation is used to relate the inner and outer velocities to the total pressure difference ΔH between the flow regions. Since the static pressure is continuous across the jet boundary

$$(1/2)\rho V_o^2 + \Delta H = (1/2)\rho V_j^2 \tag{14}$$

where V_o and V_j are the outer and jet flow speeds at the boundary. Equation (14) used with Eqs. (12) and (13) to evaluate V_o and V_j yields

$$\left[\bar{V} + \frac{\gamma_\eta}{2}\right]^2 + \frac{\gamma_\xi^2}{4} + \frac{2\Delta H}{\rho} = \left[\bar{V} - \frac{\gamma_\eta}{2}\right]^2 + \frac{\gamma_\xi^2}{4} \tag{15}$$

This equation leads to the simple result

$$\gamma_\eta = -\Delta H/\rho\bar{V} \tag{16}$$

which is analogous to the dynamic jet boundary condition of the two-dimensional analysis. Equation (16) indicates that the η component of the vorticity is coupled with the mean flow speed and the total pressure difference across the jet boundary.

The second component of the jet vortex strength γ_ξ is not directly coupled to the total pressure difference between the regions of flow. Instead it is the result of the variation of γ_η around the jet boundary in the η direction. The Helmholtz vortex law requires γ_ξ to equal the change in γ_η since a vortex filament cannot end at any point in space except at a solid boundary. This law results from the divergence of the vorticity vector being identically zero. Thus the second component of the jet vortex vector is determined from

$$\partial\gamma_\xi/\partial\xi = -\partial\gamma_\eta/\partial\eta \tag{17}$$

Of course γ_ξ is zero at all points upstream of the origin of the jet (e.g., an actuator disk).

In addition to the jet boundaries and wing surfaces, the wing trailing vortex sheet is a third surface on which boundary conditions must be specified. As demonstrated later, the trailing vortex sheet is a special case of the jet boundary and has a tangential flow boundary condition, such as Eq. (7), to be satisfied.

The field equations and boundary conditions have thus been determined for the present class of flows. The Laplacian field equations are linear and tractable, and the boundary condition on solid surfaces is that of inviscid wing aerodynamics. Additional constraints such as the Kutta condition at wing trailing edges will be imposed, depending on the type of the solid body. The jet boundary conditions, Eqs. (7, 16, and 17), introduce the two major difficulties in the wing/jet problem: the points of application of the jet boundary conditions (i.e., the jet shape) are not known a priori and Eq. (16) is nonlinear because it involves the local mean flow speed (linearization of this relation would lead to a small perturbation assumption). The first of these difficulties is a major obstacle to obtaining a solution and has been overcome in many analyses by assumption of the jet position. In the present study the jet distortion and deflection will be determined, hopefully leading to a more realistic solution.

Singularity Representation

The Laplacian velocity potential in all regions of the flowfield of the wing/jet interaction problem allows the use of potential flow methods. As in potential flow about solid bodies, the method of flow singularities embedded in a uniform stream is a powerful technique for the solution of the present problem. All solid bodies will be replaced by appropriate flow singularities such as source and vortex distributions. The type of body as well as the level of sophistication of the analysis will determine the singularities to be employed. Conventional methods such as vortex lattice analysis for wings are available to represent solid bodies. As discussed in the previous section, the jet boundary is a surface with zero normal flow but with a discontinuity in tangential flow velocity. This is, by definition, a vortex sheet and consequently, a vortex distribution is the appropriate flow singularity representation of the jet boundaries which separate the jet regions from the outer flow.

Once the solid bodies and jet boundaries have been replaced by the correct singularities, three simultaneous integral equations can be written to specify the complete system. The first integral relation results from the zero normal flow boundary condition on the surfaces of the solid bodies. The influence of the singularities of each solid body must balance the normal flow at the body surface resulting from the freestream, jet systems, and singularities of other solid bodies. A similar, second integral relation is required by zero normal flow through the jet boundaries. The third integral relation reflects the dynamic boundary condition of Eq. (16) relating the local mean flow speed along the jet boundary to the jet vortex strength. Since these relations are not explicitly required for the following method of solution, they are not discussed in detail here. Various steps of the solution procedure correspond to solving these equations in three steps. The integral equations are nonlinear but are quasi-linearized by using successive approximation within an iterative scheme.

Method of Solution

With the solid bodies and jet boundaries represented by flow singularities, solving the wing/jet interaction problem consists of determining the solid body singularity strengths and the jet boundary singularity strengths and locations. This solution cannot be obtained directly since the jet location is not known prior to determining the solution. Therefore the problem lends itself to an iterative technique.

General Iterative Technique

One iterative procedure is shown schematically by the flow chart of Fig. 2. The process begins with an initial approximate solution for the jet boundary position and jet vortex strength which determines the solid body singularity strengths by inversion of a matrix of influence coefficients with inclusion of the jet and freestream influence. This step corresponds to using the first integral equation described in the previous section. Next, the tangential flow boundary condition along the jet boundary surface, corresponding to the second integral equation of the previous section, is used to determine the jet shape. Finally the strengths of the jet singularities are determined using the dynamic pressure boundary condition, Eq. (16), or equivalently, using the third integral equation.

A convergence test consisting of comparison of the embedded singularity strengths of two successive iterations determines whether the iterative process should be continued. Following termination of this procedure, the pressures, resulting forces, and moments are calculated on the solid bodies.

Solid Body Singularities

The embedded singularity types used to represent the solid bodies in the present method are somewhat arbitrary. The combination of source and vortex singularities of Ref. 16 appears to be an adequate but complicated representation. The simpler and computationally faster vortex lattice method will

be employed presently; a higher-order, solid-body representation can be easily substituted. The accuracy of vortex lattice theory for thin airfoils is discussed in Ref. 17. Refinements of the vortex lattice method, as developed in Ref. 18 which includes the influence of bodies such as fuselages, have proven vortex lattice methods to be useful and not overly complicated. Further modifications to the vortex lattice methodology, such as inset of the lattice at the wing tip, are easily incorporated into the present structure. Basically any embedded singularity lifting surface theory can be substituted for the simple one employed presently. Thin wing-type solid bodies will be considered here initially; extensions to more general bodies are conceptually identical requiring only a modification to the vortex lattice method, such as given in Ref. 18.

The present adaptation of vortex lattice methodology is illustrated in Fig. 3 where a semispan of a wing is shown. The wing is divided into spanwise strips and chordwise divisions such that the entire lifting surface is composed of numerous quadrilateral panels which may be nonplanar. As shown in detail in Fig. 3, the upstream outboard panel is represented by a line vortex along the quarter panel line, i.e., a line connecting the points one-fourth the distance aft along each chordwise panel boundary.

In addition each panel has chordwise vortex filaments running in the surface of the wing and then extending to infinity downstream. A control point is employed for each wing panel. The location of the wing control points at the midpoint of a line connecting the points three-fourths of the distance aft along the panel side boundaries is shown to be appropriate in Ref. 17 and is presently used. The control point is the location where the solid boundary tangential flow condition, Eqs. (5) and (6), is satisfied.

The entire wing thus is replaced by a mesh of vortex filaments which extends to infinity downstream. The location of these wing and associated trailing vortex singularities is assumed to be known except for a special case, to be discussed latter, where the iterative technique is employed to determine the trailing vortex location. The calculation of the proper wing trailing vortex location is feasible for all cases, but the wake position is assumed in some cases to conserve computing time. The strengths of the wing singularities are to be determined by the solution method. The influence of the wing at any point in space is determined by evaluating the velocity induced by the vortex lattice. This is accomplished by application of the Biot-Savart law for each vortex element.

Only the velocity component normal to the surface of the wing is important since the wing boundary condition stipulates that this component is zero. The normal velocity at the control point of the ith wing panel results from three sources

$$V_{n_i} = V^{(1)}_{n_i} + V^{(2)}_{n_i}\ V^{(3)}_{n_i} \tag{18}$$

The velocities on the right-hand side of Eq. (18) are the wing and associated trailing vortex induced velocity, jet induced velocity, and freestream velocity, respectively. The wing normal self-induction can be expressed as a matrix of influence coefficients multiplied by the strength of the vortex filament of each wing panel

$$V^{(1)}_{n_i} = C_{ik}\ \Gamma_{w_k} \tag{19}$$

where Γ_{w_k} is the vortex strength of the kth wing panel. Using the tangential flow condition along the wing surface, V_{n_i} is set equal to zero and consequently by combining Eqs. (18) and (19)

$$C_{ik}\Gamma_{w_k} = -V^{(2)}_{n_i} - V^{(3)}_{n_i} \tag{20}$$

This result is a linear set of equations which determine the wing vortex strengths. The nonhomogeneous terms on the right-hand side of Eq. (20) are evaluated at each wing control point: $V^{(3)}_{n_i}$ is simply

$$V^{(3)}_{n_i} = U \cdot n_i \tag{21}$$

where U is the freestream velocity vector; $V^{(2)}_{n_i}$, the jet induced velocity, will be evaluated subsequently.

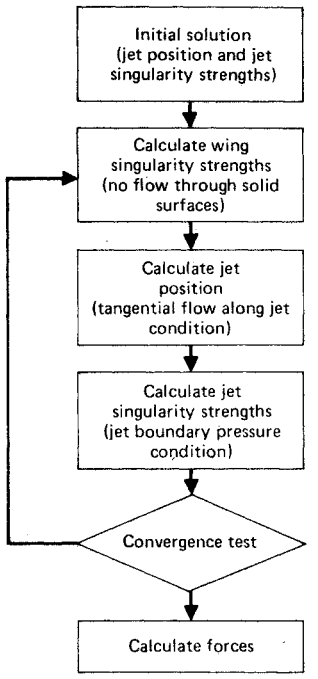

Fig. 2 Iterative scheme.

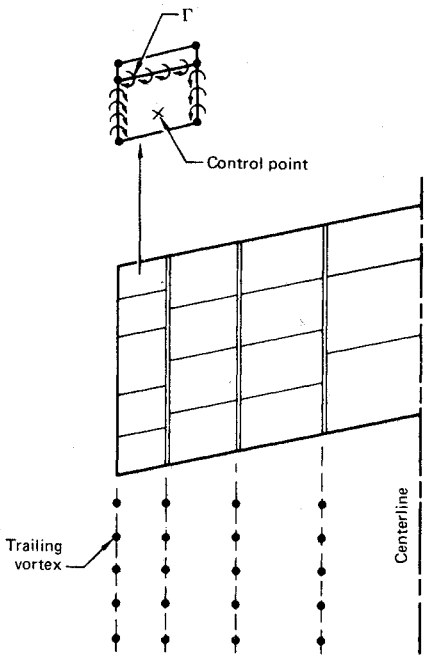

Fig. 3 Wing vortex geometry.

Jet Boundary Singularities

To evaluate the influence of the jet, a more definite jet singularity description than presented thus far is required. A jet boundary representation of about the level of approximation of the wing vortex lattice representation just discussed is illustrated in Fig. 4. Each jet boundary is divided into panels by a method similar to the procedure used for wings. The division lines run in the direction of the local velocity and end in various planes along the jet axis. Each jet boundary panel has line vortices to represent the jet vorticity in both the ξ and η directions. A jet control point is located at the midpoint of each panel.

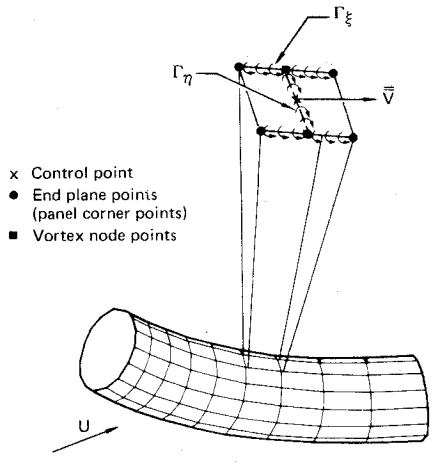

Fig. 4 Jet vorticity representation.

Jet streamwise vorticity γ_ξ is located along the panel side boundaries since these boundaries are parallel to the local velocity. The location of the jet streamwise vorticity is varied during each step of the iterative process in order that it is parallel to the average velocity vector at neighboring control points. The jet cross vorticity γ_η is in the local plane of the jet surface, but in contrast to the wing vortex lattice, γ_η is located at the mid-panel line instead of the quarter-panel position. Intuitive arguments indicate that this may be the proper arrangement of jet vorticity and control points (e.g., since γ_η results from a discontinuity in tangential velocity determined by a dynamic pressure condition, its appropriate location appears as indicated above and no forward or aft bias is indicated as in the case of wing loading and control point location). The direction of the cross vorticity must be perpendicular to the local flow vector for Eq. (16) to apply, and presently this orthogonality condition is approximated by requiring the various jet panels to end in planes which are chosen to be nearly perpendicular to the average velocity at each station along the jet axis. The filaments representing the jet cross vorticity then fall midway between adjacent endplanes and therefore are approximately perpendicular to the local velocity vector of the jet for cases of low to moderate jet deflection relative to the freestream. For cases of larger deflection a more complex geometrical adjustment of the jet cross vorticity is required during each iteration to align the vorticity more precisely in a direction perpendicular to the local velocity. Variation of the endplane directions for the current method has indicated relatively small dependency of the solutions on the exact alignment of the jet cross vorticity filaments.

With this jet boundary geometry, the mean velocity can be obtained at each jet control point

$$\bar{V}_i = \bar{V}_i^{(1)} + \bar{V}_i^{(2)} + \bar{V}_i^{(3)} \tag{22}$$

where the superscript is the same as for Eq. (18). The contribution to $\bar{V}_i^{(2)}$ because of γ_{η_k} of each panel on itself ($i=k$) is ignored. The circulation of the line vortex in the η direction can be determined using the boundary condition of Eq. (16)

$$\Gamma_{\eta_i} = -\frac{\Delta H}{\rho |\bar{V}_i|} \frac{S_i}{\ell_i} \tag{23}$$

where S_i is the jet boundary panel area and ℓ_i is the vortex filament length. At each node where a jet streamwise vortex filament intersects a cross-stream vortex line, the net vorticity is conserved according to the Helmholtz law

$$\Gamma_{\xi_{o_i}} = \Gamma_{\xi_{I_i}} - \Gamma_{\eta_i} \tag{24}$$

where $\Gamma_{\xi_{o_i}}$ is the vortex strength downstream of the ith node point and $\Gamma_{\xi_{I_i}}$ is the upstream value. Usually, at the beginning of the jet

$$\Gamma_{\xi_{I_i}}(0) = 0 \tag{25}$$

since there is no upstream vorticity. If, however, the jet is attached to a body, such as a ducted fan configuration, the values of $\Gamma_{\xi_{I_i}}(0)$ will be the trailing vortex strength at the point of attachment.

The determination of the jet boundary shape is based on the kinematic jet boundary condition of Eq. (7), which requires the local velocity vector to be tangent to the jet boundary surface. Using this result and the initial jet cross section (e.g., the actuator disk shape), a tube is determined so that the normal flow is zero along the jet boundary. In the axial direction along the jet boundary surface, the panels terminate at points which are in the same planes, called end planes. Repeated use of the tangential flow condition for each corner point around the circumference of the jet determines the panel corners successively at each panel end plane axially along the jet. This defines the jet boundary surface for each iterative step.

Since it is not practical to continue the jet shape calculation to downstream infinity, the process is terminated at a point sufficiently far downstream to limit the influence of the termination on the solid bodies in the flowfield. An approximate far-downstream jet representation, consisting of the farthest downstream calculated jet shape and vortex strength extended for several end planes, is added to the ordinary jet representation. Test calculations varying the downstream distance for the jet shape calculation have indicated that the length of the far-aft jet representation has only small influence on the upstream flowfield. This is due to two factors: the nature of vortex singularities with at least a R^{-1} decrease in induced velocity, and a self-cancelling effect resulting from the opposite sense of the jet vorticity at opposing sides of the jet boundary.

The iterative procedure can now be described using the above expressions to indicate the calculation process. Beginning with an initial guess or a previous iteration, the first step is determination of the wing singularity strengths from Eq. (20). The right-hand side of Eq. (20) is evaluated using the jet conditions of the previous iteration or starting solution. Next, Eq. (7) is used to determine a new jet shape. Finally, the jet singularity strengths are calculated by application of Eqs. (23) and (24) along the jet boundaries.

Convergence Test

After completion of these steps, a convergence test is performed to decide whether more iterations are required. An appropriate test is simply the comparison of the jet singularity strengths at corresponding points for two successive iterations or

$$E^{(\nu)} = \sum_{i=1}^{N} \frac{|\Gamma_{\eta_i}^{(\nu-1)} - \Gamma_{\eta_i}^{(\nu)}| \ell_i}{N \gamma_{\eta\infty} S_i} \tag{26}$$

where N is the number of jet vortex filaments and the superscript indicates the iteration number. Also γ_{η_∞} is a normalizing value

$$\gamma_{\eta\infty} = [(2\Delta H/\rho) + U^2]^{1/2} - U \tag{27}$$

which is the far downstream vortex strength of an axisymmetric jet obtained by setting V_o equal to U in Eq. (14) and applying the definition of vortex strength. Other calculated properties, such as the jet position, could equally well be employed to measure convergence.

Small values of $E^{(\nu)}$ indicate that the jet singularities have changed only slightly between successive iterations, and consequently the various boundary conditions are nearly satisfied at the control points.

Force Evaluation

After the iterative process has been terminated, the characteristics of the flowfield can be determined. This includes determination of flow velocities at various points in space and calculation of forces on the solid bodies. The forces on the solid bodies are determined by intergration of the surface static pressure p over each panel surface

$$F_i = -\iint_{S_i} p n dA \tag{28}$$

Using Eq. (28), the forces on each wing panel are calculated and the resulting wing lift, drag, and moments are determined by summing the contributions from all panels. To completely calculate the wing drag, a determination of the suction resulting from flow about a sharp leading edge is required using a modification to the usual vortex lattice lifting surface theory employed presently. Either a fit of the wing vortex strength to the leading edge square root behavior, or addition of a higher-order vorticity representation in a more advanced lifting surface theory would assist in determining the wing drag force. Also some vortex lattice methods use velocities evaluated at the wing vortex filaments rather than at panel control points and thereby calculate forces which are asserted to include a distributed leading-edge suction. Since the present method is not dependent on a particular lifting surface theory, modifications and substitutions to the wing representation are possible without significant alteration to the basic solution technique.

Applications

This section describes some example calculations using the present analysis. Comparisons of current solutions with previous analyses and experiments are made where possible.

Isolated Three-Dimensional Jet

The simplest application of the present calculation method is the analysis of a single jet without neighboring solid bodies. Such a jet would arise where fluid passes through an ideal actuator disk. Figure 5 illustrates the jet shape produced by an ideal actuator disk inclined at 30° relative to the freestream. The disk thrust coefficient is

$$C_T = T/\tfrac{1}{2}\rho U^2 S \tag{29}$$

where T is the force on the actuator disk

$$T = \Delta H S \tag{30}$$

and S is the disk frontal area.

The jet is observed to contract and turn toward the freestream direction. Unlike the two-dimensional case, in three dimensions the jet is not required to align itself with the freestream at downstream infinity to avoid infinite forces. Also note that the cross section of the jet, originally circular (approximated by straight line segments), becomes distorted downstream of its origin.

Wing Trailing Vortex

The most elementary combination of a jet and wing is illustrated by the wing vortex wake problem. Here the jet boundary is attached along the trailing edge of a wing and the jet total pressure differential is zero. The trailing vorticity resulting from the variation in spanwise loading of the wing is the γ_ξ value of the jet boundary and γ_η is zero since ΔH is zero. The iteration process relates the change in trailing vortex position to the variation in wing loading.

In the wing wake case the iterative process converges rapidly since the wing loading is only weakly influenced by the wake position. Figure 6 shows the resultant loading and wake shape for a rectangular planform wing of aspect ratio 6.0 at a 10° angle-of-attack. The vortex filament trajectories are indicated at four streamwise positions downstream of the wing trailing edge. Unlike the "time dependent methods" which make a one-pass calculation, the present iterative technique allows the downstream wake development to influence the upstream wake behavior and the wing loading, and vice versa.

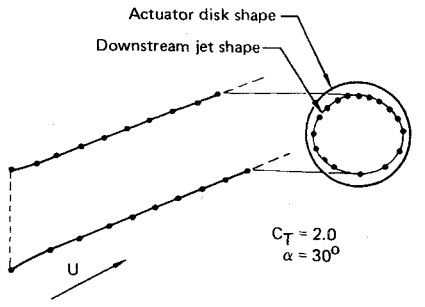

Fig. 5 Three-dimensional isolated jet.

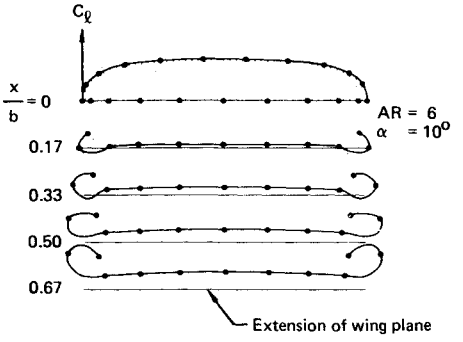

Fig. 6 Wing wake shape.

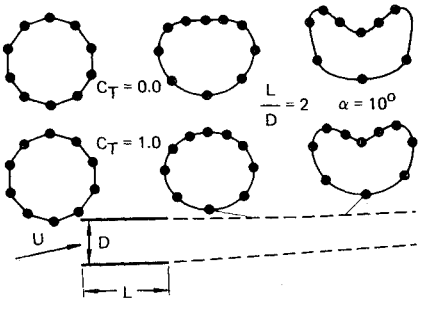

Fig. 7 Ducted fan configuration.

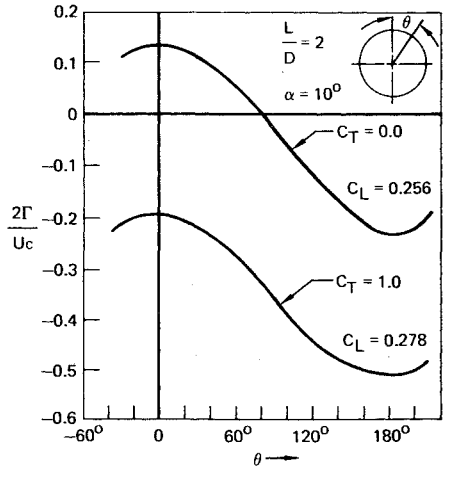

Fig. 8 Ducted fan vorticity.

Ducted Fan

The next degree of complexity beyond the trailing vortex calculation is a jet attached to a ring wing. This forms a ducted fan arrangement when ΔH is nonzero. A ring wing is formed by a vortex lattice which closes upon itself. The ring wing trailing vorticity again conforms with the position of γ_ξ for the jet. An ideal actuator is positioned within the duct

which adds a constant total pressure increment to the flow passing through the duct. This formulation indicates that the flowfield is independent of the exact position or shape of the actuator disk as long as it is positioned within the duct. The duct pressure distribution is dependent on the actuator location.

Figure 7 illustrates the present analysis of the ducted fan configuration for a circular cross-section duct with length equal to twice its diameter. The cylinder axis is at an angle of 10° with the freestream flow, and solutions for two thrust coefficient values are indicated. For $C_T=0.0$, the solution is simply a ring wing and the jet shape shown is the trailing vortex tube. The $C_T=1.0$ case corresponds to the powered ducted fan, and illustrates the change in jet shape due to thrust. Comparing the two cases of Fig. 7 shows that the cross-sectional area of the jet decreases with jet energy increase. Figure 8 shows the vortex circulation around the circumference of the duct for the two values of C_T. Here the circulation of each axial duct strip is summed and plotted against the angle around the circumference. The vortex strength for the case $C_T=1.0$ indicates a downward loading on the upper part of the duct with a larger upward loading on the lower part of the duct. The lift coefficients for the two thrust values are given, excluding the actuator contribution to lift, and an increase is indicated in lift for the powered case over the zero thrust case.

Wing and Jet Combination

The next class of example calculations, as shown in Fig. 9, involved a jet and a planar wing. Several results are presented for this case since it is an important class of flows for powered lift systems such as wing/propeller and jet augmented lift configurations. The wings in the example calculations are planar wings with rectangular planforms having neighboring circular jets. Figure 9 illustrates an example configuration with an aspect ratio 6.0 wing at 10° angle-of-attack and a jet thrust coefficient of 1.0. The actuator disk where the jet originates is located about the wing leading-edge center point, at zero incidence relative to the freestream flow.

The spanwise loadings for three values of thrust for wing/jet combinations are given in Fig. 10. The jet aspect ratio A_j is defined similarly to the wing aspect ratio.

$$A_j=2r_j/c \tag{31}$$

where r_j is the jet radius and c is the wing chord.

Also shown in Fig. 10 are results calculated by the linear method of Ref. 4. The present result generally appears to predict lower centerline loading than Ref. 4. The tip loading difference of Fig. 10 is due to the large spanwise panel size. Further attention to the influence of jet and wing panel size is required for a more complete comparison with linear results.

A final wing/jet calculation, shown in Fig. 11 provides a comparison with several other methods, as given by Rethorst.[3] The experimental data shown are from Ref. 19, one

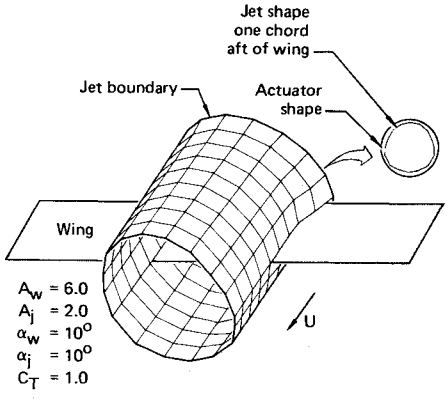

Fig. 9 Aft view of wing and jet configuration.

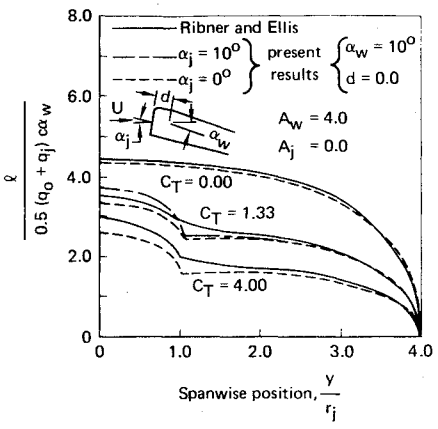

Fig. 10 Spanwise loading at various jet energies.

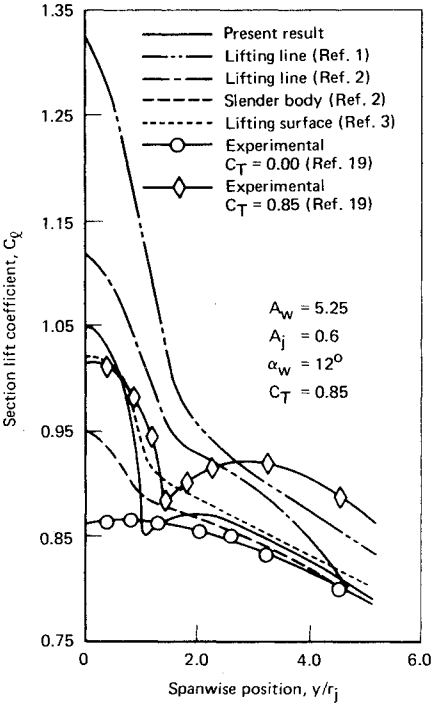

Fig. 11 Spanwise loading of wing in jet.

of the few experiments available for comparison with calculated results. The data from Ref. 19 are corrected for an estimated effect aspect ratio of 5.25 since wing end plates were used. All of the calculated results are in terms of incremental lift due to the addition of the jet, superimposed on the experimental power-off data.

Figure 11 indicates the wide range of results from various methods. This figure also shows that the experimental data just outside of the jet $y=r_j$ are significantly influenced by a viscous effect (the nacelle boundary layer) which is not included in any of the analyses shown. In addition to the nacelle boundary layer, the wing end plates walls may have significantly influenced the wing spanwise loading. Notice that the present method yields the chordwise loading, which the other methods of Fig. 11 cannot provide since they represent the wing by a single spanwise line of vorticity. Figure 12 indicates the chordwise loading at two spanwise wing locations for the experiment of Ref. 19 and the present method using a small number of chordwise wing panels to demonstrate the capability of the present method.

Multiple Wings and Jets

Unlike some previous wing/jet analyses using image techniques, the present computation method is easily applied to general configurations involving one or more wings with one or more jets. Conceptually, the present computation scheme for multiple wings and jets is exactly the same as for single wing and jet configurations since all wing and jet

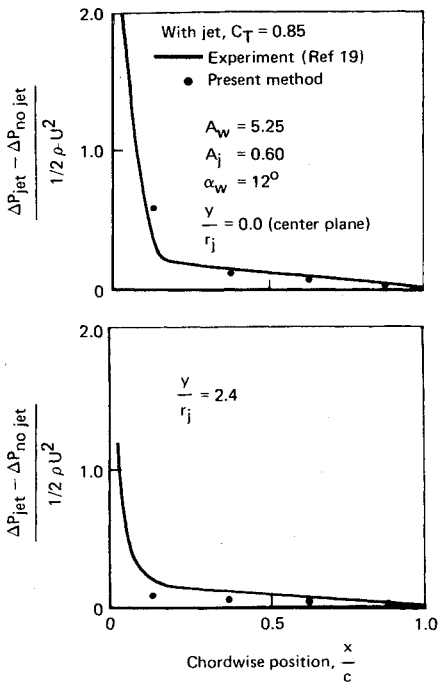

Fig. 12 Additional chordwise loading due to jet.

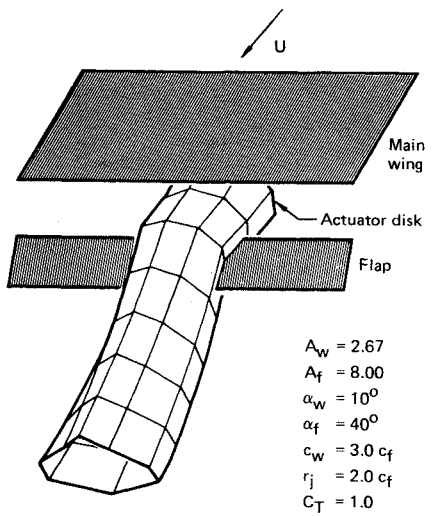

Fig. 13 Jet and multiple wing.

singularities are determined in separate steps as shown in Fig. 2. Since multiple wing and jet configurations require more wing and jet control points (because of their increased surface areas) than the single wing and jet case, computing time may be a major consideration.

To demonstrate the feasibility of calculating multiple wings with a single jet, the configuration of Fig. 13 was considered that approximates an externally blown flap high lift system. The jet boundary shape shown in Fig. 13 was calculated for the disk thrust coefficient of 1.0. A minimum of jet control points was employed for this example as indicated by the jet panels illustrated in Fig. 13 (8 circumferential panels at 7 positions along jet axis in addition to the downstream jet representation). Forty wing and flap control points were used to satisfy the tangential flow boundary condition on solid surfaces. This example further demonstrates the generality of the flow singularity formulation.

Conclusions

A three-dimensional wing/jet analysis, including the effects of jet deflection and distortion in a perfect fluid, has been presented to provide a more complete representation of the flowfield than previously available. The dynamic and kinematic jet boundary conditions have been applied by an iterative procedure to determine the proper jet vorticity and jet boundary location, thus allowing evaluation of the influence of inviscid jet distortion on neighboring solid bodies.

The results presented indicate the characteristics of solutions and the variety of configurations which can be analyzed by jet/wing interaction methodology. Reasonable correlation of the present method with previous results has been observed, but the lack of data for various configurations has severely restricted comparisons with experiments. More detailed calculations and additional test data are required to further evaluate the present approach.

The application of embedded flow singularities to replace the solid bodies and high-energy flow regions is a general method, and thus the present analysis can be modified to include jet entrainment models or to analyze additional configurations. Also the present formulation can be improved by higher-order description of the wing and jet singularities; however, the general solution technique would remain as described.

References

[1] Koning, C., "Influences of the Propeller on Other Parts of the Airplane," *Aerodynamic Theory,* Vol. IV, Springer-Verlag, Berlin, 1935.

[2] Graham, E. W., Lagerstrom, P. A., Licher, R. M., and Beane, B. J., "A Preliminary Theoretical Investigation of the Effects of Propeller Slipstream on Wing Lift," Rept. SM-14991, Nov. 1953, Douglas Aircraft Co., Long Beach, Calf.

[3] Rethorst, S. C., "Aerodynamics of Nonuniform Flows as Related to an Airfoil Extending Through a Circular Jet," *Journal of Aerospace Sciences,* Vol. 25, Jan. 1958, pp. 11-28.

[4] Ribner, H. S. and Ellis, N. D., "Theory and Computer Study of a Wing in a Slipstream," AIAA Paper 66-466, Los Angeles, Calif., June 1966.

[5] Levinsky, E. S., Thommen, H. U., Yager, P. M., and Holland, C. H., "Lifting-Surface Theory for V/STOL Aircraft in Transition and Cruise II," *Journal of Aircraft,* Vol. 7, Jan.-Feb. 1970, pp. 58-65.

[6] Mendenhall, M. R., Dillenius, M. F. E., and Spangler, S. B., "Calculation of Aerodynamic Characteristics of STOL Aircraft with Externally-Blown-Jet-Augmented Flaps," AIAA Paper 72-63, San Diego, Calif., Jan. 1972.

[7] Chang-Lu, H.-C., "Aufrollung eines zylindrischen Strahles durch Querwind," PhD. thesis, 1942, Univ. of Gottingen, Gottingen, F. R. Germany.

[8] Margason, R. J., "Analytic Description of Jet-Wake Cross Sections for a Jet Normal to a Subsonic Free Stream," SP-218, Sept. 1969, NASA.

[9] Braun, G. W., and McAllister, J. D., "Cross Wind Effects on Trajectory and Cross Sections of Turbulent Jets," SP-218, Sept. 1969, NASA.

[10] Rubbert, P. E., "Calculation of Jet Interference Effects on V/STOL Aircraft by a Nonplanar Potential Flow Method," SP-218, Sept. 1969, NASA.

[11] Monical, R. E., "A Method of Representing Fan-Wing Combinations for Three-Dimensional Potential Flow Solutions," *Journal of Aircraft,* Vol. 2, Nov.-Dec. 1965, pp. 527-530.

[12] Maskell, E. C. and Spence, D. A., "A Theory of the Jet Flap in Three Dimensions," *Proceedings of the Royal Society (London),* Series A, Vol. 251, June 1959, pp. 407-425.

[13] Lopez, M. L. and Shen, C. C., "Recent Developments in Jet Flap Theory and Its Application to STOL Aerodynamic Analysis," AIAA Paper 71-578, Palo Alto, Calif., June 1971.

[14] Shollenberger, C. A., "Analysis of the Interaction of Jets and Airfoils in Two Dimensions," *Journal of Aircraft,* Vol. 10, May 1973, pp. 267-273.

[15] Shollenberger, C. A., "An Analysis of Wings and Jets in a Inviscid and Imcompressible Fluid," Rept. MDC Q0493, June 1973, McDonnell Douglas, St. Louis, Mo.

[16] Hess, J. L., "Calculation of Potential Flow About Arbitrary Three-Dimensional Lifting Bodies," Rept. MDC J0545, 1969, McDonnell Douglas, St. Louis, Mo.

[17] James, R. M., "On the Remarkable Accuracy of Vortex Lattice Discretization in Thin Wing Theory," Rept. DAC 67211, Feb. 1969, McDonnell Douglas, St. Louis, Mo.

[18] Giesing, J. P., "Lifting Surface Theory for Wing-Fuselage Combination," Rept. DAC 67212, Vol. 1, Aug. 1968, McDonnell Douglas, St. Louis, Mo.

[19] Stuper, J., "Effect of Propeller Slipstream on Wing and Tail," TM 874, Aug. 1938, NACA.